

**Resistive effects in thin electrochemical cells. Digital
simulations of electrochemistry in electron spin resonance cells**

Ira B. Goldberg, Allen J. Bard, and Stephen W. Feldberg

J. Phys. Chem., **1972**, 76 (18), 2550-2559 • DOI: 10.1021/j100662a013 • Publication Date (Web): 01 May 2002

Downloaded from <http://pubs.acs.org> on February 19, 2009

More About This Article

The permalink <http://dx.doi.org/10.1021/j100662a013> provides access to:

- Links to articles and content related to this article
- Copyright permission to reproduce figures and/or text from this article



Resistive Effects in Thin Electrochemical Cells: Digital Simulations of Electrochemistry in Electron Spin Resonance Cells

by Ira B. Goldberg, Allen J. Bard,*

Department of Chemistry, University of Texas, Austin, Texas 78712

and Stephen W. Feldberg

Brookhaven National Laboratory, Upton, New York 11973 (Received December 6, 1971)

Publication costs assisted by Robert A. Welch Foundation and National Science Foundation

A digital simulation technique has been used to treat electrochemical reactions in a thin cell in which nonuniform current densities result from high electrolyte resistance. These calculations have been applied to conventional *in situ* electron spin resonance electrolytic cells. It has been shown that the time dependence of the esr signal is strongly dependent upon the precise electrode placement. The conventional cell is found to be unsuitable for use in pulse electrochemical-esr experiments for the measurement of kinetic parameters because secondary electrode processes can occur during a pulse and rearrangement of electrogenerated products at the electrode following the pulse must be considered. These results are also applicable to thin layer electrochemical cells, spectroelectrochemical cells, electroplating baths, and large-scale electrosynthetic cells.

Introduction

Electrochemical cells which exhibit high resistances and nonuniform current distributions include thin-layer electrochemical cells,¹ thin-layer spectroelectrochemical cells,² cells with porous electrodes,³ and *in situ* electrochemical electron spin resonance (esr) cells.^{4,5} Two kinds of resistive effects are observed with these cells. The resistance between the working electrode and the reference electrode, or the uncompensated resistance, R_u , causes the actual potential at the working electrode to be different than the measured potential by an amount iR_u where i is the current. The second resistive effect is caused by the differences in solution resistance between different points of the solution near the working electrode and the auxiliary electrode which causes different iR drops at different points parallel to the working electrode, and therefore, a nonuniform current distribution across the surface of the working electrode.

Generally, the theoretical treatments of electrochemical techniques do not consider nonuniform current densities because, in most cases, it is difficult to calculate these in closed form. Newman^{6a} and Harrar and Shain,^{6b} however, have carried out several calculations which represent situations where resistive effects cause significant nonuniform current densities and cause deviations from the usual theoretical treatments. We report here digital simulations⁷⁻⁹ of electrochemical problems involving these effects. Although the results here deal mainly with electron spin resonance cells, the techniques described should also be applicable to other electrochemical problems involving nonuniform current distributions, such as thin layer electrochemical cells, large-scale electrosynthetic cells, various electroanalytical cells, etc.

The inherent problem of high resistance in esr-electrochemical cells arises from the necessity of using only a thin layer of solution in the cavity of the esr spectrometer to avoid dielectric losses from the interaction of the microwave field with the solvent.⁴ For aqueous media, only a 0.5-mm layer of solution can be tolerated. A diagram of the conventional esr cell is shown in Figure 1a. The reference electrode cannot usually be placed near the working electrode, and thus there is considerable uncompensated iR drop between the reference electrode and the portion of the working electrode in the esr cavity. At best, the reference probe is extended to the top of the working electrode, but even here there are still significant iR drops between the segment of the working electrode closest to the reference electrode and the solution adjacent to any other segment of the working electrode.

Since cells of this design are frequently used in esr spectroscopy, it is important that the behavior of these

(1) (a) A. T. Hubbard and F. C. Anson, *Electroanal. Chem.*, **4**, 129 (1970); (b) C. N. Reilly, *Rev. Pure Appl. Chem.*, **18**, 1221 (1967), and references therein.

(2) R. W. Murray, W. R. Heineman, and G. W. O'Dom, *Anal. Chem.*, **39**, 1666 (1967).

(3) R. deLevie, *Advan. Electrochem. Electrochem. Eng.*, **6**, 329 (1967).

(4) L. H. Piette, P. Ludwig, and R. N. Adams, *Anal. Chem.*, **34**, 916 (1962).

(5) I. B. Goldberg and A. J. Bard, *J. Phys. Chem.*, **75**, 3281 (1971).

(6) (a) J. Newman, *Electroanal. Chem.*, **6**, in press; (b) J. E. Harrar and I. Shain, *Anal. Chem.*, **38**, 1148 (1966).

(7) S. W. Feldberg, *Electroanal. Chem.*, **3**, 199 (1969), and references therein.

(8) K. B. Prater and A. J. Bard, *J. Electrochem. Soc.*, **117**, 209, 335, 1517 (1970).

(9) S. W. Feldberg in "Applications of Computers to Chemical Instrumentation," J. S. Mattson, H. P. Mark, Jr., H. C. MacDonald, Jr., Ed., Marcel Dekker, New York, N. Y., and references therein.

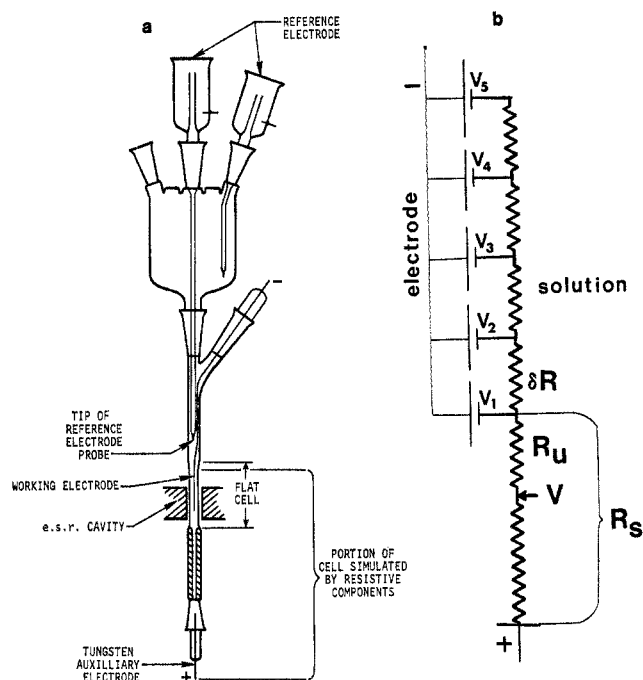


Figure 1. (a) Diagram of conventional esr-electrochemical cell. (b) Schematic representation of a thin-layer electrochemical cell. V_i represents the potential at the center of electrode segment i .

cells is understood. To this date, very little work concerning this aspect of the electrogeneration of radicals has been presented. We present here a semi-quantitative study of this type of cell using the simplest model possible. The conditions which are selected for this calculation are: (1) each of the charge-transfer steps is nernstian; (2) the double-layer capacitance is negligible; (3) there are no adsorbed species; (4) there is no deposition of material at the electrode and the diffusion coefficients of all species are nearly equal; (5) at the beginning of the simulated experiment the entire solution consists of the neutral species of the electroactive material; (6) the cell can be represented as shown in Figure 1b and (7) convection is negligible. These conditions appear to describe the electrochemical behavior of the majority of systems of organic compounds in nonaqueous solvents studied by esr. Modifications to include slow electron-transfer steps, coupled homogeneous chemical reactions, double-layer charging, etc., can be included in the simulation using procedures previously described;⁷⁻⁹ however, since our aim is to demonstrate difficulties in behavior even under the simplest conditions, we do not deal with these additional complications here.

Digital Simulation

Simulations of electrochemical processes are discussed in detail by Feldberg.⁷ To incorporate the differing resistances to different parts of the working electrode, as well as the finite cell thickness, some modifications must be made in the procedures of the pre-

vious simulations involving uniform current densities and semiinfinite linear diffusion. Details of the method employed are given in the Appendix and only an outline of the procedure is given here. The model chosen to represent the electrochemical cell is shown in Figure 1b.

Rather than considering a cell in which the reference electrode is above the working electrode, as shown in Figure 1a, we chose to consider the reference electrode adjacent to the lower edge of the working electrode. This system is more amenable to the method of digital simulation and provides a suitable reference point for later discussion. The total resistance between the counter electrode and the end of the working electrode is R_s . The total electrolysis current, I , flows through R_s . The resistances between different higher segments along the working electrode and the counter electrode are given by $R_s + \delta R$, $R_s + 2\delta R$, etc. The fraction of the total current flowing into each segment of the working electrode is given by δi_1 , δi_2 , etc., so that

$$I = \sum_{k=1}^{N_{\max}} \delta i_k \quad (1)$$

where N_{\max} is the number of segments of the working electrode. It is further assumed that the resistance across the double layer is negligible. The cell thickness is simulated by a finite number of solution layers, 1, 2, ..., N_{lim} , where N_{lim} is the number of increments of thickness. The model is used for the case of a single working electrode with the nonconducting cell wall terminating diffusion, such as the usual esr cell (Figure 2).

If the length of each electrode segment is much larger than the increment of cell thickness, then the cell may be treated as a series of smaller, independent cells, and diffusion between the vertical solution elements can be neglected. This lateral diffusion can be included in the calculation if necessary.

The current of the k th element, δi_k , depends upon

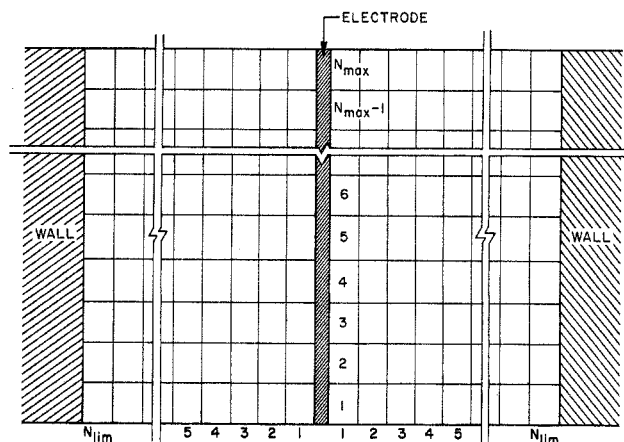


Figure 2. Digital representation of thin electrochemical cell.

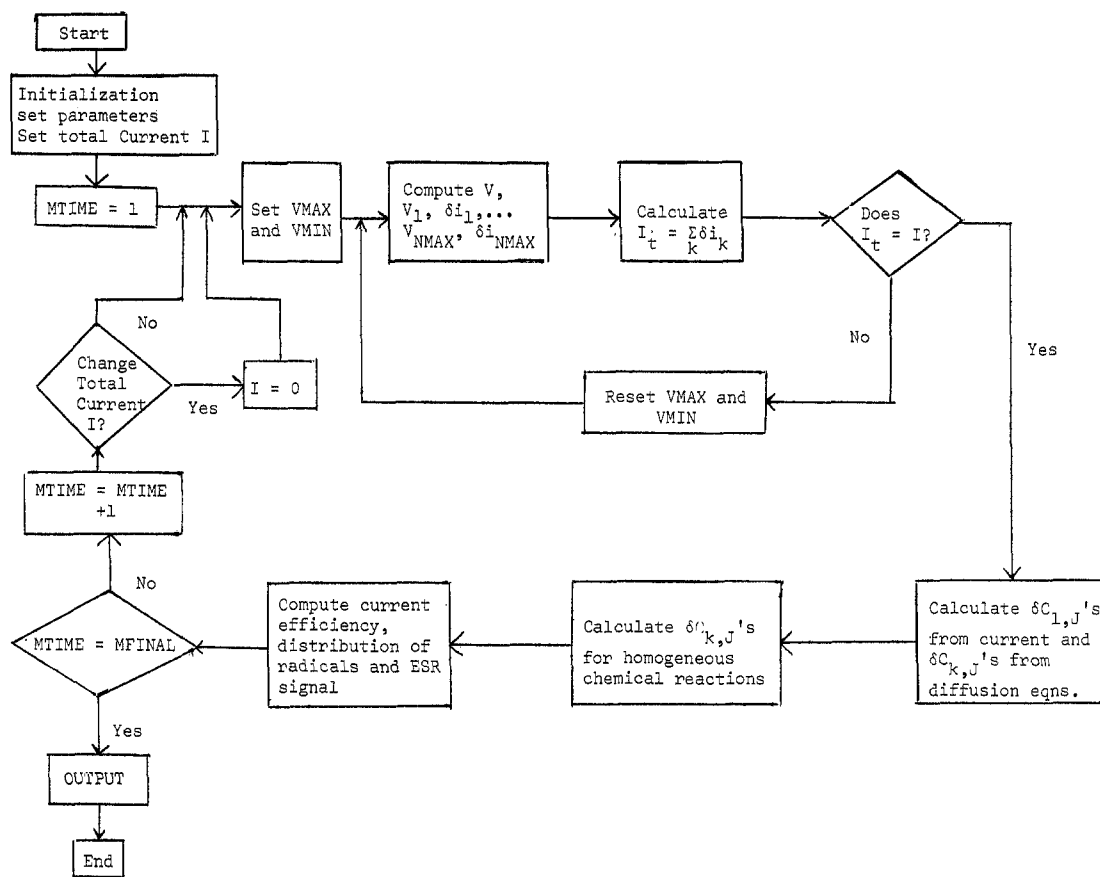


Figure 3. Flow chart of digital simulation program.

the potential of that element, V_k . To determine the potential V_k , it is necessary to determine the potential of the first element of the electrode, V_1 , and then determine the other potentials by computing the voltage drops between the elements. Since these voltage drops depend upon δi_k , an iterative procedure is used to find the V_k 's and the δi_k 's which satisfy the resistive drops along the electrode and also satisfy eq 1. Note also that V_1 differs from V by the amount iR_u . The iterative method employed to calculate V was the bisection method.¹⁰ In this method, reasonable positive and negative limits of V , denoted V_{\max} and V_{\min} , are guessed. The first trial value of V is taken as $\frac{1}{2}(V_{\max} + V_{\min})$, and values of δi_k and V_k are calculated for all segments of the electrode. The total current, *via* eq 1, is then determined. If this current is too large, V_{\min} is replaced by V , or if the current is too small, V_{\max} is replaced by V , and the calculations are repeated until the desired degree of convergence is obtained. A flow chart of the program is shown in Figure 3.

Either parallel plate or single electrode systems with potential or current step processes can be treated by this method. The only difference among them is that the boundary conditions are slightly different. Details of these simulations are given in the Appendix.

Experimental Section

Simulations of In Situ Electrolysis in ESR. Two aspects of electrochemical generation of radical ions in esr were investigated with these calculations. The first problem was to examine the effects of solution resistance and electrode placement in the microwave cavity during continuous electrolysis, and the second was to investigate the feasibility of pulse experiments in conventional esr electrolysis cells, such as the Varian V-4556 or E246 (cell dimensions $4 \times 0.9 \times 0.05$ cm), Bruker BER-400 2E or the Jeolco JES-ELIO cell.

In continuous generation of radical ions in esr, several effects have been noted: (1) the rate of increase of the initial esr signal varies considerably between experiments; (2) during electrolysis, the esr signal reaches a peak after a certain time and then diminishes; (3) there may be a sudden increase of the esr signal when the current is stopped; and (4) the esr signal due to even stable radicals often decreases shortly after the current is stopped.

A characteristic system which may be used as an

(10) H. M. Lieberstein, "A Course in Numerical Analysis," Harper and Row, New York, N. Y., 1968, pp 3, 6; A. Ralston, "A First Course in Numerical Analysis," McGraw-Hill, New York, N. Y., 1965, p 495; R. W. Hamming, "Numerical Methods for Scientists and Engineers," McGraw-Hill, New York, N. Y., 1962, p 352.

illustration of the behavior of electrogeneration in esr is that of anthraquinone. The half-wave potentials of anthraquinone in dimethylformamide (DMF) are -0.83 and -1.40 V vs. sce¹¹ for the first and second waves, respectively. In aprotic media both the anion and dianion are stable. Typical of the solvents used in esr studies are dimethylformamide (DMF) and 1,2-dimethoxyethane (DME) with 0.1 M supporting electrolyte. The specific resistances of these solvent systems are about 250^{12} and 4000 ohm-cm,¹³ respectively.

The sensitivity in the microwave cavity of the spectrometer is not uniform. In an unloaded cavity of the TE 102 and TE 104 modes, the signal S resulting from a paramagnetic sample distributed inside the cavity will follow an expression of the form^{14,15}

$$S = A \int_0^z \cos^2 \left(\frac{\pi}{2} \left(\frac{y}{z} - 1 \right) \right) N(y) dy \quad (2)$$

where z is the height of the cavity (for x band, $z = 2.290$ cm), y is the distance from the bottom of the cavity, $N(y)$ is the number of radicals at y , and A is the proportionality constant which depends upon the instrumental conditions and upon the degeneracy and line width of the paramagnetic material. Although the presence of the cell, the solution, and the electrode and the use of field modulation will cause some deviation of the signal from that predicted by eq 2, it is still accurate enough for our purposes. It is also useful to treat the proportionality constant as unity. In this way, when all of the radicals are located at the center of the cavity, the signal will equal the number of radicals. After the calculation of the concentrations in each of the volume elements (see Appendix), $N(y)$ is determined by adding the number of radicals in all of the volume elements in each vertical level. A digital form of eq 2 is used in the calculation.

In most electrolytic cells which have been used for *in situ* generation, the reference electrode is not near the working electrode and as a result, the uncompensated resistance is extremely high. Even though the electrolysis is carried out under controlled potential conditions, the high uncompensated voltage drop effects an essentially constant current generation.⁵

Consider the simulation of the generation of the anthraquinone anion radical for 100 sec at $100 \mu\text{A}$ in a 2.5 mM anthraquinone solution in DMF where the electrode dimensions are 0.5×3 cm and the cell thickness is 0.05 cm. The length of the electrode was divided into 25 sections and the experiment duration into 200 time units. The counter electrode is located below the esr cell and outside the cavity. Figure 4 shows the relative current distribution at several times during the electrolysis. Initially ($t = 0$) all of the current is used to produce the radical at segments of the electrode closest to the counter electrode. Shortly afterward ($t = 25$ sec), the dianion is formed near the lower edge of the working electrode, while the anion

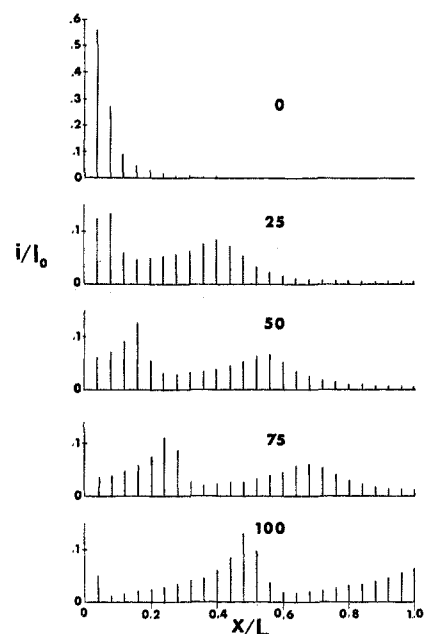


Figure 4. Simulation results showing fraction to total current at different segments of the working electrode at various times during the constant current electrolysis of 2.5 mM anthraquinone in 0.1 M tetrabutylammonium iodide-dimethylformamide solution: total current $100 \mu\text{A}$; electrode width, 0.5 cm; length, 3.00 cm. Time of electrolysis (sec) given above distribution diagram. Bars represent current at the center of each segment.

is generated further up. Two current peaks are evident from the diagram. At longer times, the peaks move further along the electrode as the electroreducible material is depleted ($t = 50$ to 75 sec, respectively). During the last time unit shown, solvent decomposition begins as the potential of the first element of the electrode becomes sufficiently negative.

Curve R of Figure 5a shows the relative quantity of radicals during the generation, where the maximum amount of radicals is normalized to 1. In addition, the esr signal is shown for several different electrode placements. Curve A shows the esr signal when the edge closest to the counter electrode is located at the point of maximum sensitivity in the cavity, that is at the center of the cavity [$(z - y_0)/z = 1/2$ where z is the height of the cavity and y_0 is the lower edge of the electrode]. Curve B represents the esr signal when the lower edge is placed $z/4$ above the bottom of the cavity, and curve C represents the esr signal when the bottom of the electrode is at the bottom of the

(11) P. H. Given, M. E. Peover, and J. M. Schoen, *J. Chem. Soc.*, 2764 (1958).

(12) F. K. Andryushchenko, K. G. Parfenova, and O. A. Slotin, *Sov. Electrochem.*, **2**, 689 (1966); D. S. Reid and C. A. Vincent, *J. Electroanal. Chem.*, **18**, 427 (1968), and references therein.

(13) Estimated from the measurements of C. Carvajal, K. J. Tolle, J. Smid, and M. Szwarc, *J. Amer. Chem. Soc.*, **87**, 5548 (1965).

(14) B. Kastening, *Ber. Bunsenges. Phys. Chem.*, **72**, 20 (1968).

(15) C. P. Poole, Jr., "Electron Spin Resonance," Interscience, New York, N. Y., pp 263-270.

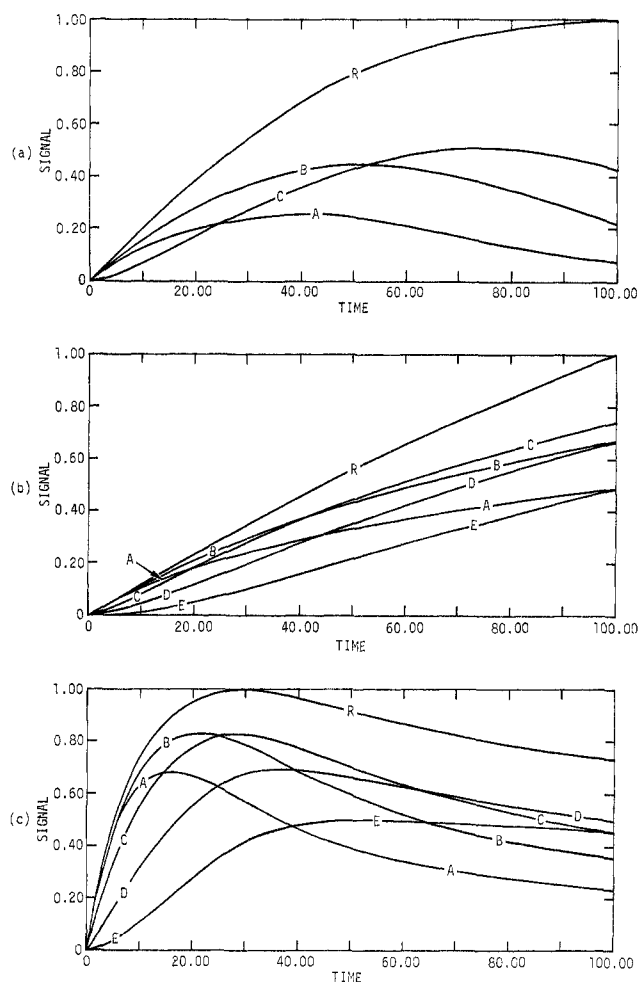


Figure 5. Simulation results showing the quantity of radical (R) and the esr signal vs. time for various placements of the working electrode. See text for description of electrode placements. Concentration of electroactive material is 2.5 mM: a, specific resistance of solution 250 ohm-cm; stable anion and dianion, cf. Figure 4, current 100 μ A; b, specific resistance of solution = 4000 ohm-cm; stable anion and dianion, $E_{1/2} = -0.83$ V, -1.40 V, current 50 μ A; cathodic limit 50 μ A at -3 V; c, specific resistance of solution is 4000 ohm-cm; no dianion is generated. $E_{1/2}$ of reduction to anion = -0.83 V, rate of decomposition of anion is 0.125 sec^{-1} , cathodic limit 50 μ A at -3 V.

cavity. Several differences between these curves are immediately apparent. Initially, the most rapid rise of the esr signal will be when the edge of the electrode is at the center of the cavity, but during a long electrolysis, this positioning gives rise to the smallest signal. When the electrode is placed $z/4$ of the distance above the bottom cavity (curve B), the rise of the esr signal is nearly as rapid, but after 4 sec the signal is more intense than in the position corresponding to curve A. Under the conditions represented by curve C, at the start of the electrolysis, the radicals are generated at the bottom of the electrode. This produces a very small esr signal, and consequently the rise of the signal is very slow. At longer times the

radicals at the edge of the electrode are depleted due to further reduction to the dianion. When the electrode is at the center of the cavity (curve A), the esr signal will decrease, but this will have a smaller effect upon the signal when the bottom of the electrode is below the center (curves B or C). When the electrode is at these positions, represented by B and C, the material near more of the electrode is detected by the spectrometer, and as a result of the movement of the current waves up the electrode, the signal represented by B reaches a maximum before that represented by C.

Figure 5b shows a similar constant current generation for a solution of 2.5 mM anthraquinone in the higher resistance solvent DME. The only differences are that the cell thickness was 0.1 cm, and that the current was 50 μ A. Because of the higher resistance, the electrochemical reactions are confined to the lower portions of the electrode. Curves A, B, C, D, and E show the signals obtained when the bottom edge of the electrode is placed at $z/2$, $3z/8$, $z/4$, $z/8$, and 0 cm above the bottom of the cavity. The total amount of radicals is shown by curve R. As before, the initial rise of the esr signal is greatest when the lower edge of the electrode is placed at $z/2$. Here, however, the greatest signal will occur when the edge of the electrode is placed $z/4$ above the cavity floor because the total electrolytic reaction occurs over a smaller portion of the electrode than that shown in Figure 5a.

Figure 5c shows the same conditions of electrogeneration as Figure 5b, except that there it is assumed the dianion is not formed, and the radical is assumed to decompose in a first-order process when the rate constant is about 0.125 sec^{-1} . The apparent signal-time curves are significantly dependent upon the precise electrode position, and the rate of decomposition. A similar problem was found by Kastening¹⁴ when using electrochemical flow systems in esr for the measurement of kinetic parameters.

Simulations of In Situ Current Pulse Experiments. In order to carry out pulse electrolytic experiments to measure the stability of radicals, it is necessary to use moderately high currents, depending upon the lifetime of the radical. The anthraquinone-DMF system was again chosen as an ideal system to represent this process. The conditions simulated were the same as for the previous constant current generations in DMF, except that the length of the electrode in this case was 1.15 cm (equal to $z/2$) and the current pulse was 1 mA for 0.5 sec. The concentration of anthraquinone was 5 mM. Under these conditions, and if semiinfinite linear diffusion were possible, then the transition time for a 1 e process would be 0.43 sec. Using a 2.3-cm electrode so that the transition time is longer does not significantly alter the shape of the curve because the reaction is still localized mostly at the bottom of the electrode.

Figure 6 shows the current distributions at several

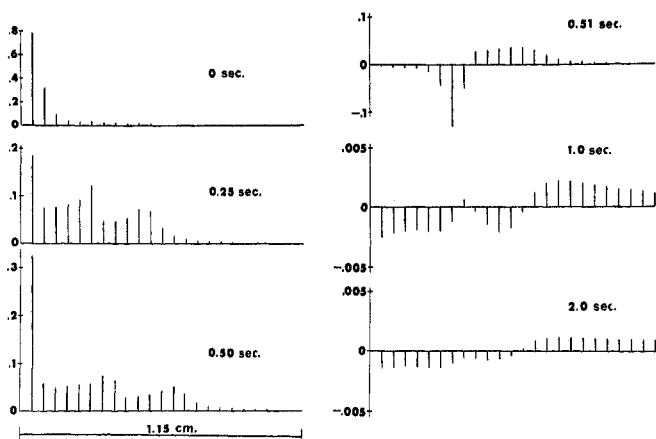


Figure 6. Simulation results showing fraction of current at different segments of the working electrode during and following a short current pulse. Bars represent current at the center of each segment of the electrode. Solution 5.0 *M*; current 1.0 mA; pulse duration = 0.50 sec; specific resistance 250 ohm-cm; $D = 10^{-5}$ cm²/sec; half-wave potentials -0.83 V and -1.40 V; background current = 1 mA at -3.00 V; electrode size 0.5 cm \times 1.15 cm.

times during and following the current pulse. At the instant of application of current the entire current is used in the production of the anion. After about 0.02 sec some dianion is produced. By $t = 0.25$ sec a large portion of the current goes toward the generation of the dianion and about 11% goes toward solvent decomposition. Thus, 100% current efficiency for the generation of anion cannot be maintained for an appreciable fraction of the transition time. At $t = 0.50$ sec a much larger portion of current goes toward production of the dianion and solvent decomposition. At the end of the 0.5-sec pulse, the *net* current efficiency for generation of the anion is about 65%. It should also be mentioned here that the anthraquinone-DMF system is close to ideal for definition of the electrochemical waves, because there is 0.57 V difference between the first and second waves, and about 1.3 V between the second wave and the cathodic limit for solvent decomposition. If the first and second waves were closer together and the cathodic limit was not so far removed, then the current efficiency would be much less than obtained here.

After the current is stopped, the iR drops between elements which have been changing throughout the pulse are sharply reduced. Still, however, the potential established by the $R^{2-}-R^-$ and $R^- - R$ couples would be different along the electrode unless current is allowed to flow within the electrode, enabling redistribution of R^{2-} , R^- and R at the electrode surface. The current distribution immediately following the pulse is shown in Figure 6, where $t = 0.51$ sec. Observe that at the bottom of the electrode there is an anodic current, indicating that R^{2-} is oxidized to R^- , while at the end of the electrode R is reduced to R^- .

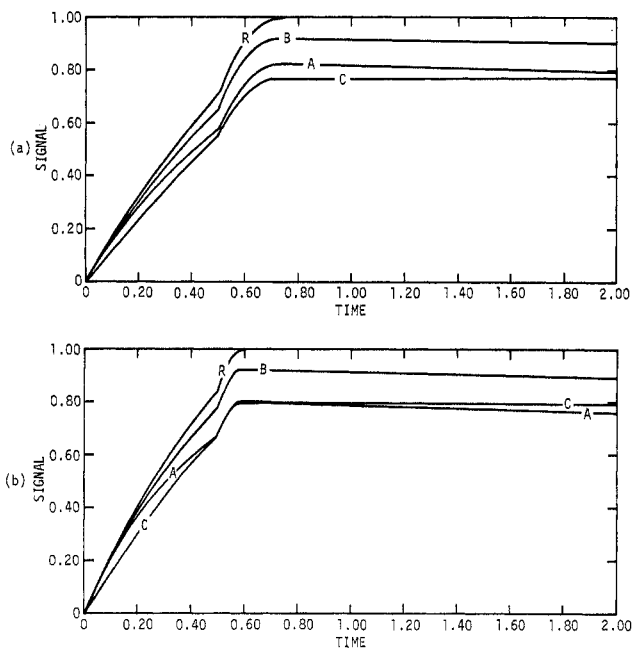


Figure 7. Quantity of radicals (R) and esr signal for different electrode placement *vs.* time during and following a 0.50-sec pulse. See text for description of electrode placements. Same parameters simulated as in Figure 6: a, stable anion and dianion; b, stable anion; dianion decomposes in a first order process $k = 5$ sec⁻¹.

This internal current is quite large until the dianion is nearly exhausted from the solution either by current flow or by reacting with neutral R to form $2R^-$. After this, however, there are still gradients of R and R^- adjacent to the electrode. This causes a smaller current which tends to equalize the relative amounts of these species. Thus, R^- is oxidized to R at the first elements of the electrode and R is reduced to R^- at the last elements [Figure 6 ($t = 1.0, 2.0$)]. The esr signal which results from this system is shown in Figure 7a. As before, the curve marked R represents the amount of radicals in the cell. Curves A, B, and C represent electrode placements where the edge of the electrode is $Z/2$, $3Z/8$, and $Z/4$ above the bottom of the cavity. As before, the most rapid increase of the signal occurs when the edge of the electrode is in the most sensitive region of the cavity. However, because dianion is produced first at the edge of the electrode, this position does not give the maximum signal. When the current is stopped, the amount of radical in solution increases rapidly as does the esr signal because of the internal current. However, even after the amount of radicals present reaches a steady state (curve R approaches 1), the esr signal still changes. In curves A and B there is a noticeable decrease in the esr signal as radicals are removed from a more sensitive region and generated in a less sensitive region. Curve C, on the other hand, exhibits a small increase of signal (about 0.3% from $t = 0.8$ sec to $t = 2$ sec) because in this case, radicals are removed from a position which

gives rise to a smaller signal and are regenerated at a position which gives rise to a larger one (cf. Figure 6). When the conventional electrode is used, such as the longer 3-cm gauze electrode supplied with commercial cells,¹¹ the decrease of the esr signal after the current pulse is considerably greater than shown here, especially when the edge of the electrode is placed at the center of the cavity. In cases where the dianion is not stable, the rise of the signal after the pulse is stopped is considerably less pronounced, as shown in Figure 7b. In this simulation the dianion was assumed to have a first-order decomposition rate of $k = 5 \text{ sec}^{-1}$.

Effects similar to those discussed here have been observed experimentally for both constant current and current pulse experiments (Figure 8a and b). Figure 8a shows a solution of anthracene electrolyzed at 0.5 mA for 100 sec in DMF. Since the dianion is unstable, only a small rise is seen when the current is stopped. Also, because the radical may be slightly unstable in DMF, the decrease of the esr signal is more rapid than expected. Figure 8b shows a solution of anthraquinone generated for 120 sec. A very rapid rise of the esr signal and then a slow decay is observed. These experiments were carried out in the conventional cell.

The results of these calculations show that due to the high resistance in the cell, secondary electrode processes may occur even before the transition time of the first electrode process. Since in long term generation there is probably a significant amount of convection with the cell, the actual experimental system will exhibit a greater current efficiency for production of a radical than that calculated here. The results of these calculations also indicate that even if it were possible to place a reference electrode adjacent to the lower edge of the working electrode and the potential here maintained on the plateau of the reduction to the radical, the potential on the upper portions of the electrode would still be much more positive, and although R^{2-} should not be formed, there would still be a galvanic effect between R and R^- at different areas of the electrode surface when the circuit was opened. Thus, the conventional esr cell would not be suitable for pulse experiments.

Conclusions

These calculations have indicated several problems which are inherent in electrogeneration of radicals for esr. First of all, pulse experiments are not easily carried out in conventional esr cells because of the change of the iR drop during and following the applied pulse, so that the amount of radicals adjacent to different parts of the electrode are redistributed after the pulse. Conceivably, an electrode could be constructed of a material which would produce an electrode resistance such that the resistance of the solution between the bottom of the electrode and a point adjacent to the

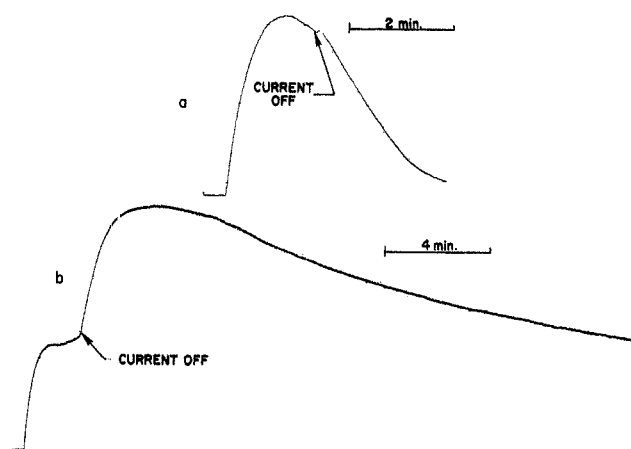


Figure 8. Experimental signal-time curves: a, 5 mM anthracene in 0.1 M tetrabutylammonium iodide-dimethylformamide solution for 100 sec generation at 100 μA ; results typical of unstable dianion; b, 5 mM anthraquinone generated under same conditions for 120 sec; results typical of stable anion radical and dianion.

electrode would be the same as the resistance of the electrode between the top of the electrode and that point on the electrode. Although this would permit a uniform current density over the electrode surface, this design would have poor qualities as an electrochemical cell. On the other hand, the counter electrode and reference electrode may also be placed in the flat portion of the electrochemical cell so that both uniform current densities and good cell characteristics would be attainable.⁵ The electrode size and placement in the esr experiment is critical to the intensity and time dependence of the esr signal. The optimum parameters for a given solvent system must be chosen experimentally. In the highest resistive media, the edge of the electrode is best placed in the region just below the center of the cavity where the sensitivity is greatest because the electrolysis occurs over a fairly small region of the electrode. On the other hand, if an extremely high current is used when the edge of a long electrode is placed at the bottom of the cavity, and assuming that no secondary radicals are produced, then the desired radical may be generated at more sensitive regions of the spectrometer so that an esr signal can be observed.

With solutions of lower resistance, the current becomes more uniform, and the optimum signal is obtained when the electrode is placed deeper into the cavity. Similarly, as the current becomes greater, the zone where radicals are produced moves farther up the electrode.

An interesting effect was observed in these simulations. If only one electrochemical process was assumed to occur and allowing semiinfinite diffusion, then regardless of the electrical resistance of the medium, the chronopotentiometric transition time was constant. Here the transition time must be defined as the time

when the surface concentration of R, in the reaction $R + e \rightarrow R^-$, becomes zero over all regions of the electrode.

Acknowledgment. The support of the National Science Foundation (GP6688X) and the Robert A. Welch Foundation is gratefully acknowledged. The electron paramagnetic resonance spectrometer was purchased under a grant from the National Science Foundation (GP2090). Part of this work was performed under the auspices of the U. S. Atomic Energy Commission.

Appendix

Digital Simulation. The models for digital simulation of electron transfer, homogeneous kinetics, and semiinfinite diffusion have been discussed in detail.⁷ Because in many cases the cells described here are thinner than the effective diffusion layer in semiinfinite linear diffusion, the treatment of diffusion must be slightly modified. In order to simulate diffusion to a planar electrode, the solution is divided into layers parallel to the electrode surface. In thin cells, the solution must be divided into an integral number of equal volume elements between the electrode and the wall as shown in Figure 2.

For semiinfinite diffusion the number of volume elements that must be considered in the simulation is⁷

$$M_{\text{lim}} = 6\sqrt{D_m M_t} \quad (\text{A1})$$

where M_{lim} is the number of segments of length perpendicular to the electrode, D_m is the diffusion parameter used in the simulation (0.40 has been chosen here) where we have assumed that the diffusion coefficients of all species are equal, and M_t is the number of time units desired in the simulation. Equation A1 corresponds to

$$\delta = 6\sqrt{Dt} \quad (\text{A2})$$

where δ is the diffusion layer thickness, D is the diffusion coefficient, and t is the total time of the experiment. From (A1) and (A2)

$$\delta = M_{\text{lim}} \sqrt{\frac{DT}{D_m M_t}} \quad (\text{A3})$$

In thin cells, diffusion must be constrained within the cell walls. Using a relationship similar to (A3), the number of volume elements, N_{lim} in a thin layer cell of thickness l is given by

$$N_{\text{lim}} = l \sqrt{\frac{D_m M_t}{Dt}} \quad (\text{A4})$$

The number of volume elements which must be used in the simulation is, therefore, the minimum value of N_{lim} and M_{lim} . In the program D_m is adjusted to make the right side of (A4) an integer.

To account for the different current densities at dif-

ferent portions of the electrode, the electrode is divided into N_{max} segments (indexed by I) as shown in Figure 2. The length of the electrode segment is not related to the length of the volume element normal to the electrode. The number of segments selected depends upon the degree of precision desired and the resistance of the solution. Diffusion perpendicular to the electrode (between layers of $k = 1$ and $k = N_{\text{lim}}$) is treated by finite difference forms of Fick's equations.⁷ The relative concentration of the j th species in box $I, k, F_j'(I, k)$ because of diffusion occurring during one time increment, for $k = 2$ to $N_{\text{lim}} - 1$ is⁷

$$F_j'(I, k) = F_j(I, k)(t) + D_m[F_j(I, k-1) - 2F_j(I, k) + F_j(I, k)] \quad (\text{A5})$$

where $F_j(I, k)$ is the relative concentrations of species j at the end of the preceding time increment. In the cell such as diagrammed in Figure 2 for box $k = N_{\text{lim}}$ the relative concentration is

$$F_j'(I, N_{\text{lim}}) = F_j(I, N_{\text{lim}}) + D_m[F_j(I, N_{\text{lim}} - 1) - F_j(I, N_{\text{lim}})] \quad (\text{A6})$$

For box $k = 1$, any amount of substance j generated at the electrode surface must be added to the concentration of box 1. Assume $J_j(I)$ is the flux of species j electrogenerated at element I of the electrode. The concentration in boxes $k = 1$ is then given by

$$F_j'(I, 1) = F_j(I, 1) + D_m[F_j(I, 2) - F_j(I, 1)] - J_j(I) \quad (\text{A7})$$

where we neglect lateral diffusion.

If the electron-transfer reactions are assumed to be nernstian and the diffusion coefficients of all of the species are equal, then the flux of each species may be calculated in the following way. The electrode is assumed to be at the edge of the first box. Since the flux is proportional to the concentration gradient, and the concentration in the simulation represents the concentration at the center of that box, then the flux is given by

$$J_j(I) = D_m[F_j'(I, 1) - F_j^0(I)]/0.5 \quad (\text{A8})$$

where $F_j^0(I)$ is the relative concentration of species j at the electrode surface. The factor 0.5 enters (A8) because the distance between the electrode surface and the center of box $k = 1$ is $1/2$ of the unit length of each box. The relative surface concentrations of each species are given by the Nernst equation

$$\frac{F_1^0(I)}{F_2^0(I)} = \exp\left\{\frac{F}{RT}[E(I) - E^{0'}]\right\} \quad (\text{A9})$$

where the potential $E(I)$ is the potential of segment I and $E^{0'}$ is the standard potential. Since the total flux at the electrode surface must be zero, if there is no accumulation of material at the surface, then

$$\sum_{j=1}^{N_s} J_j(I) = 0 \quad (\text{A10})$$

where N_s is the number of species in the solution. Equations A8 through A10 can be solved simultaneously with the elimination of the parameters $F_j(I)$ and from this the flux of each species and the current at each electrode segment can be calculated as a function of potential. Diffusion between horizontal layers can be neglected because the length of each segment of the electrode given by h/N_{\max} , where h is the overall length of the electrode, is smaller than $6\sqrt{Dt}$.

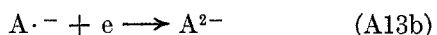
Constant Current Steps: ESR and Thin-Layer Cells. We assume that a current of magnitude i is passed through the cell. This may be converted to a dimensionless parameter Z_t which corresponds to the flux, given by

$$Z_t = \frac{iN_{\max}}{FCwh} \frac{tD_m}{DM_t} \quad (\text{A11})$$

where F is the Faraday, C is the experimental concentration, and w and h are the width and length of the electrode. If the current parameter at each element I of the electrode is given by $Z(I)$ then during a constant current experiment

$$Z_t = \sum_{I=1}^{N_{\max}} Z(I) \quad (\text{A12})$$

For a reduction, the following electrode reactions contribute to $Z(I)$



where A is electroactive substance and S is solvent or supporting electrolyte. For simplicity, we have assumed that the reactions in (A13a) and (A13b) are Nernstian and (A13c) is irreversible. Species A is denoted as $j = 1$, $A \cdot^-$ as $j = 2$, and A^{2-} as $j = 3$. The current due to the reduction of species A is given by $J_1(I) - J_3(I)$.⁷ The current due to the decomposition of solvent is denoted by $Z_b(I)$. Therefore, the current at element I of the electrode becomes

$$Z(I) = J_1(I) - J_3(I) + Z_b(I) \quad (\text{A14})$$

To include the resistance between segments of the electrode, the parameter used to represent the resistance must be made compatible to the dimensionless parameters representing the potential and the current. Thus, the resistance R_m between each segment of solution at the electrode surface, as shown in Figure 1, is given by

$$R_m = \left[\frac{\sigma h i F}{l w N_{\max} Z R T} \right] \quad (\text{A15})$$

where σ is the specific resistance and RT is 2.4777×10^3 J at 298°K. The first term in (A15) is the resistance between electrode segments. The uncompensated resistance is represented in a similar way except

that the value of R_u is substituted for the bracketed term of (A15).

In order to determine the measured potential, V , the bisection method¹⁰ was used. The most positive possible value of the potential, V_{\max} , and the most negative possible value, V_{\min} , are selected. The first guess for the measured potential is

$$V = 0.5(V_{\max} + V_{\min}) \quad (\text{A16})$$

From the value of V , the potential of the first segment of the electrode $E(1)$ is calculated

$$E(1) = V + Z_t R_u \quad (\text{A17})$$

and from this value, $Z(I)$ is calculated. Since the current flowing beyond the first electrode segment, Z_r is $Z_t - Z(1)$, the potential at the second electrode segment is given by

$$E(2) = E(1) + Z_r R_m = V + Z_t R_u + Z_r R_m \quad (\text{A18})$$

From this, the current in segment 2, $Z(2)$, is calculated. The procedure is repeated for all N_{\max} segments. The currents of all electrode segments are then totalled and compared to Z_t . If the total current is too large, then V_{\min} is replaced by V , and if the current is too small, V_{\max} is replaced by V . The procedure from (A16) is repeated until the total current is within a certain error of Z_t . A flow chart of the computer program is given in Figure 3.

A word of caution is necessary in using this method of calculation. Convergence of the calculated value of the total current to Z_t is very rapid when high currents are simulated. In the case of low currents, however, such as in thin layer electrochemical cells or zero current following a current pulse as in the esr cells, it is often necessary to use double precision to calculate $Z(I)$ from V , V_{\max} , V_{\min} , and the half-wave potentials. The 14 decimal digits carried by the CDC 6600 and CDC 6400 computers are often not sufficient to obtain a convergent value. This effect becomes most pronounced at zero current when many electrode elements are used in the calculation.

Nomenclature

1. Dimensional Variables.

- δ = distance perpendicular to the electrode, cm
- C = concentration, mol/cm³
- D = diffusion coefficient, cm²/sec
- i = current, A
- t = time, sec
- h = length of working electrode, cm
- w = width of working electrode, cm
- l = cell thickness, cm
- F = Faraday's constant, 96,500 Coul/equiv
- σ = specific resistance, ohm-cm

2. Indices

- I = index of segment of working electrode
- j = index of species: $j = 1$, A; $j = 2$, A⁻; $j = 3$, A²⁻
- k = index of length segment perpendicular to working electrode

3. Variables			
N_s	= number of electroactive species	$J_j(I)$	= fractional flux of species j at the surface of segment I of the working electrode current due to background reactions
N_{\max}	= number of segments of working electrode	$Z_b(I)$	= current due to background reactions at segment I of the working electrode
M_{lim}	= number of segments of length required to represent semiinfinite linear diffusion	Z_t	= total current
N_{lim}	= number of segments of length required to represent cell thickness	$E(I)$	= potential measured between segment I of the working electrode and the reference electrode
M_t	= number of time increments of the calculation	$E^{0'}$	= standard formal potential
D_m	= diffusion parameter used in finite difference equations	R_m	= resistance (dimensionless) between solution segments at the surface of the electrode
$F_j'(I,k)$	= fractional concentration of j in the center of the segments of coordinates (I,k) after applying finite difference equations	R_u	= uncompensated resistance
$F_j(I,k)$	= same as $F_j'(I,k)$ but before application of finite difference equation	V	= trial potential
$F_j^0(I)$	= fractional concentration of j at the surface of segment I of the working electrode	V_{\max}, V_{\min}	= positive and negative limits of potential

Irreversible Potentiometric Behavior of Isotactic Poly(methacrylic Acid)¹

by J. C. Leyte,* H. M. R. Arbouw-van der Veen, and L. H. Zuiderweg

Gorlaeus Laboratories, Department of Physical Chemistry, University of Leyden, Leyden, The Netherlands
(Received February 7, 1972)

Experimental evidence is presented for the irreversibility of the potentiometric titration curve of isotactic poly(methacrylic acid). A description in terms of thermodynamically irreversible conformation changes is given and it is shown that the dissipation due to the transition of a monomeric unit is independent of its state of dissociation.

In recent literature,² some attention has been given to irreversible behavior of macromolecular systems because of the implicit importance of these phenomena in the quest for molecular mechanisms for information storage. It has been pointed out³ that hysteresis loops in physical-chemical properties of macromolecules offer, at least in principle, the possibility of storing, on a molecular level, information about the history of the system.

The investigated macromolecular systems are, however, rather complicated from a physical-chemical point of view: RNA from several sources, mixtures of poly A and poly U, etc. In all these systems complicated chemical equilibria as well as polymer conformational equilibria shift simultaneously as a function of the driving physical variable (usually pH). We wish to report the occurrence of hysteresis in a relatively simple polyelectrolyte molecule, poly(methacrylic acid) (PMA).

Experimental Section

Isotactic poly(methyl methacrylate) (PMMA) was synthesized according to the standard procedure.⁴ Molecular weights were estimated from intrinsic viscos-

ities of the CHCl_3 solutions using the relation $[\eta] = 4.8 \times 10^{-5} (\bar{M}_v)^{0.80}$ given by Goode.⁵ For the polymer used in this investigation we found $\bar{M}_v = 3.9 \times 10^5$.

The tacticity of the PMMA was determined from nmr spectra (100 MHz) of CHCl_3 solutions, run at 60°. The signals from the α -methyl group showed an isotactic triade content of 95–98%.

Hydrolysis of the ester was achieved by dissolving 6 g of the dry ester in 300 ml of oxygen-free 96% H_2SO_4 solution. After maintaining the system for 10 hr at room temperature the ester was dissolved. The temperature was raised to 60°; after 2 hr the solution was cooled to 0° and 1.2 l. of distilled water was added to the yellow solution. After filtering and washing, the

(1) Dedicated to Professor Dr. H. Veldstra on the occasion of his retirement from the chair of Biochemistry of the University of Leyden.

(2) A. Katchalsky, "International Symposium on Macromolecules, Leiden, 1970," Butterworths, London, 1971, p 368.

(3) A. Katchalsky, A. Oplatka, and A. Litan in "Molecular Architecture in Cell Physiology," T. Hayashi and A. G. Szent. Györgyi, Ed., Prentice-Hall, New York, N. Y., 1966, p 3.

(4) G. C. Overberger, *Macromol. Syn.*, 1, 29 (1963).

(5) W. E. Goode, F. H. Owens, R. P. Fellemann, W. H. Snijder, and J. E. Moore, *J. Polym. Sci.*, 46, 321 (1960).